arXiv:1907.12607v1 [cond-mat.mes-hall] 29 Jul 2019

Polaritonic Molecular Clock: All-Optical Ultrafast Imaging of Wavepacket Dynamics without Probe Pulses

R. E. F. Silva,[1,*] Javier del Pino,[2] Francisco J. García-Vidal,[1,3] and Johannes Feist[1,†]

[1]*Departamento de Física Teórica de la Materia Condensada and Condensed Matter Physics Center (IFIMAC), Universidad Autónoma de Madrid, E-28049 Madrid, Spain*

[2]*Center for Nanophotonics, AMOLF, Science Park 104, 1098 XG Amsterdam, The Netherlands*

[3]*Donostia International Physics Center (DIPC), E-20018 Donostia/San Sebastián, Spain*

Conventional approaches to probing ultrafast molecular dynamics rely on the use of synchronized laser pulses with a well-defined time delay. Typically, a pump pulse excites a wavepacket in the molecule. A subsequent probe pulse can then dissociates or ionizes the molecule, and measurement of the molecular fragments provides information about *where* the wavepacket was for each time delay. In this work, we propose to exploit the ultrafast nuclear-position-dependent emission obtained due to large light-matter coupling in plasmonic nanocavities to image wavepacket dynamics using only a single pump pulse. We show that the time-resolved emission from the cavity provides information about *when* the wavepacket passes a given region in nuclear configuration space. This approach can image both cavity-modified dynamics on polaritonic (hybrid light-matter) potentials in the strong light-matter coupling regime as well as bare-molecule dynamics in the intermediate coupling regime of large Purcell enhancements, and provides a new route towards ultrafast molecular spectroscopy with plasmonic nanocavities.

INTRODUCTION

The interaction of light and matter is one of the most fundamental ways to unveil the laws of nature and also a very important tool in the control and manipulation of physical systems. When a confined light mode and a quantum emitter interact, the timescale for the energy exchange between both constituents can become faster than their decay or decoherence times and the system enters the strong coupling regime [1–3]. In this regime, the excitations of the system become hybrid-light matter states, so-called polaritons, separated by the vacuum Rabi splitting Ω_R. Due to their relatively large dipole moments and large exciton binding energies, strong coupling can be achieved with organic molecules at room temperature down to the few- or even single-molecule level [4–6]. Strong coupling can lead to significant changes in the behavior of the coupled system, affecting properties such as the optical response [3–12], energy transport [13–16], chemical reactivity [17–25], and intersystem crossing [22, 26, 27]. However, up to now these setups did not provide direct information on the molecular dynamics.

A well-known approach to directly probe molecular dynamics is through the use of ultrashort coherent laser pulses, pioneered in the fields of femtochemistry [28] and attosecond science [29]. This allows to observe and control nuclear and electronic dynamics in atoms and molecules at their natural timescale (fs and sub-fs) and is a fundamental tool towards a better understanding of chemical and electronic processes [28–34]. In particular, real-time imaging of molecular dynamics can be achieved in experiments with a pump-probe setup with femtosecond resolution combined with the measurement of photoelectron spectra [31]. While similar approaches could in principle provide a dynamical picture of molecules under strong light-matter coupling [35–37], common molecular observables (such as dissociation or ionization yields or photoelectron spectra) are difficult to access in typical experimental setups, with molecules embedded in a solid-state matrix and confined within nanoscale cavities [4–6].

In this article, we demonstrate that the ultrafast emission induced by strong coupling to plasmonic modes can be used to monitor molecular wavepacket dynamics by measuring the time-resolved light emission of the system after excitation by an ultrashort laser pulse, without the need of a synchronized probe pulse. Our approach exploits the fact that the light-matter hybridization in a molecule is nuclear-position-dependent. Consequently, efficient emission only occurs in regions where the polaritonic potential energy surface (PoPES) [18, 38] on which the nuclear wavepacket moves possesses a significant contribution of the cavity mode, as sketched in Figure 1. Additionally, due to the very low lifetime (or equivalently, low quality factor) of typical plasmonic nanocavity modes on the order of femtoseconds, emission from the cavity also becomes an ultrafast process. Instead of using a probe pulse to learn *where* the nuclear wavepacket is at a given time delay, we thus use the nuclear-position-dependent emission to learn *when* the wavepacket passes a given spatial region. Tracking the time-dependent emission from the cavity then gives direct information about the nuclear dynamics by effectively clocking the time it takes the wavepacket to perform a roundtrip in the PoPES through an all-optical measurement. We note that a variety of experimental techniques allow the measurement of time-dependent electric fields with femtosecond resolution, e.g., SPIDER [39], FROG [40] or d-scan [41].

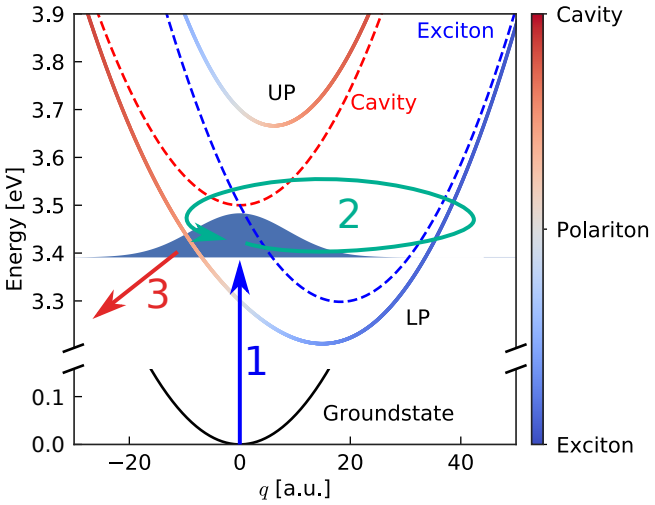

Figure 1. Polaritonic potential energy surfaces (PoPES) in the single-excitation subspace for a single molecule coupled to a confined light mode. The red dashed line represents the uncoupled potential energy surfaces (PES) for a ground-state molecule with a single photon in the cavity, while the blue dashed line represents the molecular excited-state PES with no photons present and the black solid line represents the ground-state PES of the molecule. The solid blue/gray/red curves are the lower and upper polariton PES, with the color encoding the excitonic/polaritonic/photonic character as a function of nuclear position q. The filled blue curve represents the vibrational ground-state wavefunction of the electronic ground-state PES. The arrows represent the excitation by the laser pulse (1), oscillatory motion of the excited vibrational wavepacket (2) and radiative emission (3).

RESULTS

We illustrate these ideas using a minimal model system: A single-mode nanocavity containing a molecule with two electronic states and a single vibrational degree of freedom, which for simplicity we approximate as a harmonic oscillator (with displacement between the ground and excited state due to exciton-phonon coupling). Our model is then equivalent to the Holstein-Jaynes-Cummings model that has been widely used in the literature to model strongly coupled organic molecules [19, 42–44], with the main difference that we explicitly treat cavity losses and driving by an ultrashort (few-fs) laser pulse, and monitor the time-dependent emission. While this is a strongly reduced model which allows for a straightforward interpretation, we will later show that the results we observe are also obtained in realistic simulations of molecules with a plethora of vibrational modes leading to rapid dephasing [10]. The system is described by the Hamiltonian (setting $\hbar = 1$)

$$H(t) = \omega_e \sigma^+\sigma^- + \frac{p^2}{2} + \omega_v^2 \frac{q^2}{2} - \lambda_v \sqrt{2\omega_v}\sigma^+\sigma^- q + \omega_c a^\dagger a + \frac{\Omega_R}{2}(a^\dagger\sigma^- + a\sigma^+) + \mu_c E(t)(a^\dagger + a), \quad (1)$$

where σ^+ (σ^-) is the raising (lowering) operator for the electronic state with excitation energy $\omega_e = 3.5$ eV, while p and q are the mass-weighted nuclear momentum and position operators for the vibrational mode with frequency $\omega_v = 0.182$ eV and exciton-phonon coupling strength $\lambda_v = 0.192$ eV (with these parameters we reproduce the properties of the anthracene molecule, see Methods for further details). The cavity is described through the photon annihilation (creation) operators a ($a^\dagger$), with a photon energy chosen on resonance with the exciton, $\omega_c = \omega_e$. In addition to the coherent dynamics described by the Hamiltonian, the cavity mode decays with rate $\gamma_c = 0.1$ eV, described by a standard Lindblad decay operator (see Methods for details). The photon-exciton coupling is described through the Rabi splitting at resonance, $\Omega_R = 2\vec{E}_{1\mathrm{ph}}(\vec{r}_m) \cdot \vec{\mu}_{eg}$, where $\vec{E}_{1\mathrm{ph}}(\vec{r}_m)$ is the quantized mode field of the cavity at the molecular position, and $\vec{\mu}_{eg}$ is the transition dipole moment of the molecule (in principle, this is q-dependent, but is taken constant here for simplicity). Finally, the cavity mode is coupled through its effective dipole moment μ_c to an external (classical) laser pulse $E(t) = E_0 \cos(\omega_L t) \exp(-\sigma_L^2 t^2/2)$, with central frequency ω_L and spectral bandwidth σ_L.

We start by analyzing the system response in the strong-coupling regime ($\Omega_R = 0.4$ eV) after excitation by an ultrashort laser pulse with $\sigma_L = 0.1$ eV, while scanning the laser frequency ω_L. The laser intensity is chosen small enough to remain in the single-excitation subspace (i.e., within linear response). In Figure 2, the time-dependent radiative emission intensity, E_R (proportional to the cavity photon population $\langle a^\dagger a \rangle$) and the exciton population, $\langle \sigma^+\sigma^- \rangle$, are shown. We observe that when the laser pulse is resonant with the lower polariton region, i.e. for ω_L between 3.2 and 3.5 eV, the cavity emission is modulated in time with a period of around 26 fs, while no such oscillation is observed when the upper polariton branch is excited for ω_L between 3.5 and 3.8 eV. This behavior can be understood with the help of the PoPES, shown in Figure 1. They are obtained by treating nuclear motion within the Born-Oppenheimer approximation, i.e., with q treated as an adiabatic parameter (see Methods for details). Within the Franck-Condon approximation, short-pulse excitation creates a copy of the vibrational ground-state (centered at $q = 0$) on the relevant polaritonic PES. This vibrational wavepacket will then evolve on the potential surface, performing oscillatory motion, with the character of the wavepacket also oscillating between photon-dominated and exciton-dominated depending on nuclear position. However, as radiative emission of the cavity mode is orders of magnitude faster than from the bare molecule (typically, femtoseconds compared to nanoseconds), efficient emission is only possible in regions where the relevant PoPES has a significant photon contribution. Focusing first on the lower polariton, this condition is fulfilled for $q < 0$ for the parameters chosen here, explaining the observed temporal modulation of the emission intensity, which effectively

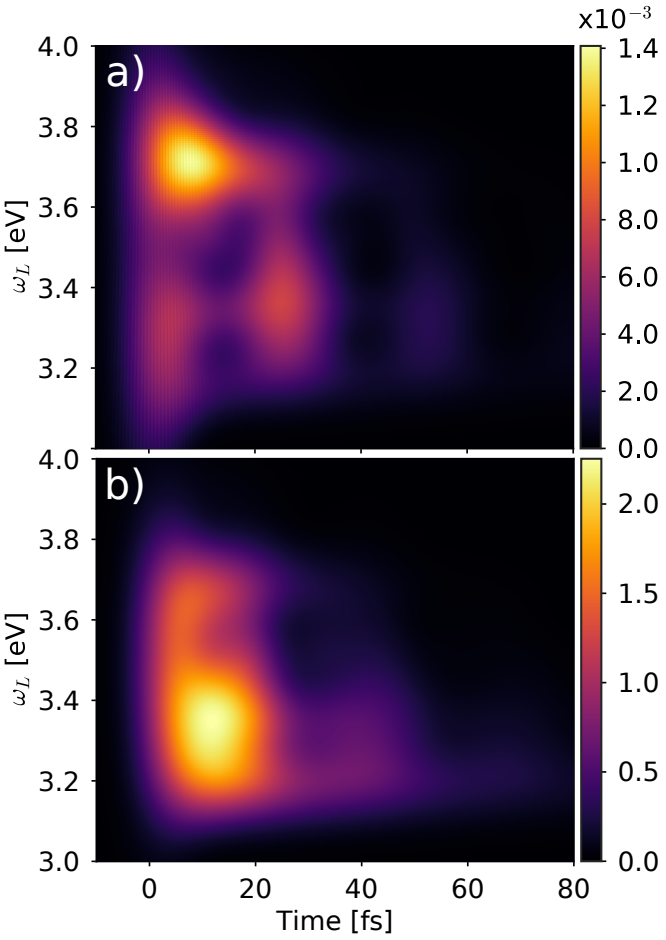

Figure 2. Mean values of the time-dependent radiative emission, E_R, (a) and $\langle\sigma^+\sigma^-\rangle$ (b) for different values of ω_L and for $\Omega_R = 0.4$ eV. For all calculations, $E_0 = 2.1 \times 10^{-7}$ a.u. and $\sigma_L = 0.1$ eV.

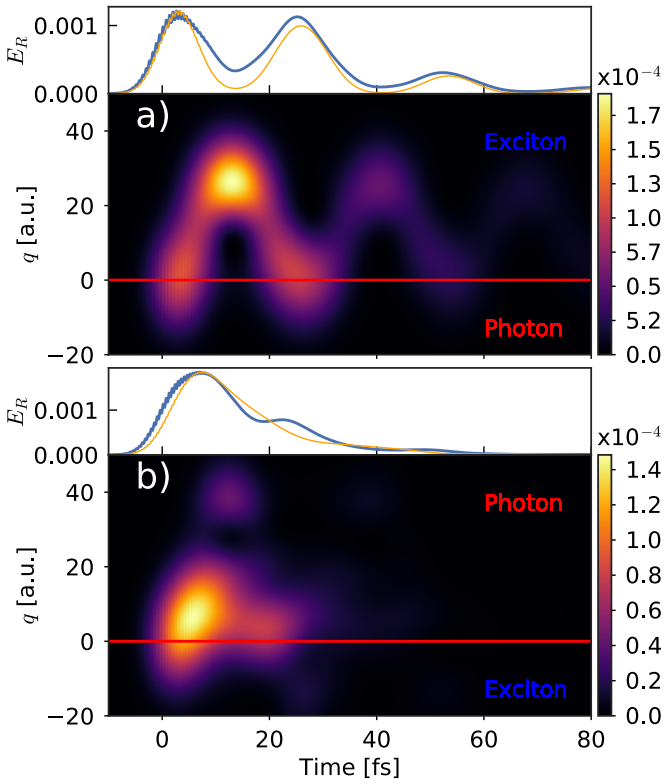

Figure 3. Probability density of the vibrational wavepackets in the single-excitation subspace for two different laser frequencies: (a) $\omega_L = 3.3$ eV and (b) $\omega_L = 3.7$ eV. The red line at $q = 0$ indicates the border where the polariton switches from photonic to excitonic character for the (a) lower and (b) upper polariton. The upper panels in each subfigure show the time-dependent emission from the cavity (thick blue lines) and the (scaled) probability of the nuclear wavepacket on the photonic side, given by $q < 0$ for (a) and $q > 0$ for (b) (orange lines). For both calculations, $E_0 = 2.1 \times 10^{-7}$ a.u. and $\sigma_L = 0.15$ eV.

corresponds to clocking of the nuclear wavepacket motion. Furthermore, the period of this motion is determined by the curvature of the lower polariton PoPES, which is different to the bare-molecule oscillation period $T_v \approx 22.7$ fs. Fitting the lower polariton curve to a harmonic oscillator for the current parameters gives an oscillation period of 25.9 fs, in excellent agreement with the observed modulation frequency of 26 fs. The temporal emission modulation thus also provides a direct fingerprint of the strong-coupling induced modifications of molecular structure. On the other hand, excitation to the upper polariton creates a wavepacket that spends most of its time in the region with efficient emission ($q > 0$ for the upper PoPES), such that no clear oscillation between photonic and excitonic character, and thus no modulation in the emission intensity, is observed.

Up to now, we have confirmed that molecular dynamics imprints its fingerprint in the time-dependent radiative emission of the cavity. We now demonstrate that the time-resolved emission intensity indeed provides a direct quantitative probe of the nuclear wavepacket dynamics. In Figure 3, we show the nuclear probability density $|\psi(q)|^2$ in the single-excitation subspace under resonant excitation of the lower polariton, Figure 3(a), and upper polariton, Figure 3(b), respectively. For case (a), the wavepacket starts periodic motion around the minimum of the lower polariton curve, $q_{\min} \approx 15$ a.u., after the initial excitation at $t \approx 0$. In the upper panel, we show E_R and the probability to find the nuclei at $q \leq 0$, given by $\int_{-\infty}^{0} |\psi(q)|^2 \mathrm{d}q$. The observed good agreement demonstrates that it is possible to track the position of the nuclear wavepacket in time through the emission from the cavity. The similarly good agreement found in Figure 3(b), with the integral this case performed for $q \geq 0$ corresponding to excitation of the upper polariton branch reinforces this notion. We again observe that less pronounced oscillation is observed for excitation of the UP branch. We also note that for case (b), there is a small contribution of the lower polariton to the excitation (since this is energetically still allowed), explaining the slightly worse agreement between the full

calculation and the simplified approximation based on integrating the nuclear probability density.

We next investigate the dependence of the effects discussed above on the Rabi splitting Ω_R, focusing in particular on the case of smaller Ω_R, including within the weak-coupling regime. The corresponding time-resolved radiative emission E_R is shown in Figure 4(a) on a logarithmic scale. Since we have observed the lower polariton branch to display more interesting dynamics, the central laser frequency is chosen such that the lower polariton branch is excited for each Rabi frequency, i.e., $\omega_L = \omega_e - \Omega_R/2$. Several regimes can be clearly distinguished: For small coupling, $\Omega_R \lesssim 0.03$ eV, the molecules barely participate in the dynamics and the response is dominated by the excitation and subsequent ringdown (with time constant $\tau_c = \hbar/\gamma_c \approx 6.6$ fs) of the bare cavity mode (green line in Figure 4(b)). In contrast, within the strong-coupling regime, $\Omega_R \gtrsim 0.10$ eV, the previously discussed oscillations can be seen, with the modulation frequency increasing concomitantly with Ω_R due to the increasingly large modification of the polaritonic PES and thus the nuclear oscillation period (blue line in Figure 4(b)). For intermediate values of Ω_R, a slightly different behavior is observed: emission occurs over relatively long times, but is again modulated over time, with a period of around 23 fs, in good agreement with the bare-molecule vibrational period, $T_v \approx 22.7$ fs. This can be understood by examining the molecular PES in the case of weak coupling, as shown in Figure 4(c). In that case, the potential energy surfaces are almost unmodified and the initial laser pulse only excites the cavity mode, but the relatively large coupling is sufficient to allow efficient energy transfer to the molecule (exactly in the Franck-Condon region) within the lifetime of the cavity mode, such that the emission is not fully dominated by the cavity response. The molecular wavepacket then again oscillates, now within the bare molecular excited-state PES. However, for nuclear configurations where the molecular exciton and the cavity mode are resonant (within the cavity bandwidth), the molecular radiative decay is enhanced strongly through the Purcell effect, leading to ultrafast emission exactly when the nuclear wavepacket crosses the resonant configuration ($q \approx 0$ for the parameters considered here). In the intermediate coupling regime, it is important to point out that the oscillations will be more clear when the cavity has an ultrafast decay. This can be seen when comparing the radiative emission for two different decay rates, $\gamma_c = 0.1$ and 0.3 eV (solid red and dashed dark red lines in Figure 4(b)), where the oscillations are more prominent for more lossy cavities. We note that the more relaxed requirements for Ω_R in this intermediate regime should make it more easily accessible in controlled experimental setups [6].

We next discuss the requirements that must be fulfilled for the phenomena described above to be observed. We first mention that while we have used harmonic

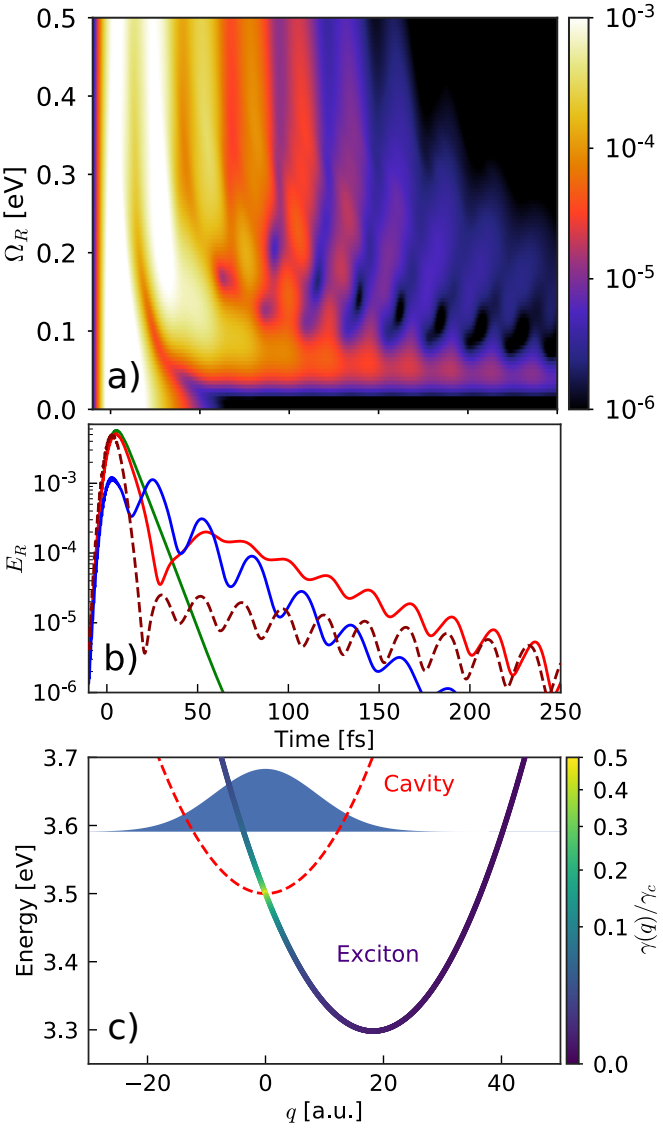

Figure 4. (a) Time-dependent radiative emission from the cavity, E_R, for different values of Ω_R and laser frequency resonant with the bare lower polariton energy, $\omega_L = \omega_e - \Omega_R/2$. For all calculations, $E_0 = 2.1 \times 10^{-7}$ a.u. and $\sigma_L = 0.15$ eV. (b) Same as in (a) for three different values of $\Omega_R = 0.01,\ 0.07$ and 0.4 eV(green, red and blue lines respectively). The dashed dark red line represents the case for $\Omega_R = 0.07$ eV and a cavity with larger decay rate, $\gamma_c = 0.3$ eV. (c) Potential energy surfaces in the weak-coupling regime with large Purcell enhancement of the emission. The red dashed line represents the PES of the molecule in its ground-state with a photon in the cavity. The blue-yellow solid line represents the molecular excited-state PES with no photons present, with the position-dependent (Purcell-enhanced) decay rate encoded in the purple/yellow color scale. The filled blue curve represents the vibrational ground-state wavefunction of the electronic ground-state PES.

oscillator vibrational potentials for simplicity, this is not a requirement and, indeed, anharmonic PES could lead to more complex/interesting observed emission dynamics. However, the molecule needs to have sufficiently strong exciton-phonon coupling (i.e., a sufficiently large change in the q-dependent excitation frequency) to lead to significant spatial modulation of the cavity and exciton components of the PoPES. Furthermore, the slope of the (polaritonic) PES in the Franck-Condon region has to be large enough for the nuclear wavepacket to leave the initial position before it has time to decay completely (although this problem could be mitigated by, e.g., choosing the cavity to be resonant in another region of nuclear configuration space instead of at the equilibrium configuration). For the Holstein-type molecular model studied here, these conditions are satisfied if λ_v is comparable to the vibrational frequency ω_v, and both are comparable to the cavity decay rate γ_c. These properties are fulfilled for several organic molecules that have been used in strong-coupling experiments, such as anthracene [45] or the rylene dye [N,N0-Bis(2,6-diisopropylphenyl)-1,7- and -1,6-bis(2,6-diisopropylphenoxy)- perylene-3,4:9,10-tetracarboximide] [46]. Additionally, in order to be able to observe coherent wavepacket motion, internal vibrational relaxation and dephasing, which typically occurs on the scale of tens to hundreds of femtoseconds in solid-state environments, must be slow enough compared to the dynamics of interest. In the Methods section, we demonstrate that this is the case for the anthracene molecule by comparing the Holstein-Jaynes-Cummings-model calculation with large-scale quantum dynamics simulations including all vibrational modes of the molecule, performed using the time-dependent variational matrix product state (TDVMPS) approach [10, 47].

To summarize, we have proposed a novel scheme to probe and image molecular dynamics by measuring the time-dependent radiative emission obtained after short-pulse excitation of a system containing a single molecule and a nanocavity with large light-matter coupling, close to or within the strong-coupling regime. We show that this approach enables to retrieve a direct mapping of nuclear wavepacket motion in the time domain. In the strong-coupling regime, this gives access to the cavity-modified molecular dynamics occurring on the PoPES, while in the weak-coupling regime, it allows probing of the bare-molecule excited-state dynamics. By exploiting the ultrafast emission dynamics in typical highly lossy plasmonic nanocavity, we obtain the time-resolved dynamics without the need for a pump-probe setup with synchronized femtosecond pulses. In addition, in contrast to the common approaches of femtochemistry, our proposed scheme does not require direct access to molecular observables such as photoelectron spectra or fragmentation yields, which are difficult to obtain for typical experimental geometries. Instead, it only relies on optical access to the nanocavity mode. Additionally, the scheme only depends on the properties of the first few electronic states of the molecule, and is not affected by, e.g., the multitude of ionization channels that have to be taken into account in photoionization [34]. Finally, since only a single excitation is imparted to the molecule and the dynamics are probed through the photons emitted upon relaxation to the ground-state, the molecule is left intact after the pulse. At the same time, this implies that the absolute photon numbers to be measured are small. This could be mitigated by using high-repetition-rate sources (readily available for the low laser intensities required), as well as collecting the response from an array of identical nanocavities, taking advantage of highly reproducible setups available nowadays, e.g., through DNA origami [6, 48].

METHODS

The time dynamics is described by the following Lindblad master equation

$$\dot{\rho}(t) = -i[H(t), \rho(t)] + \gamma_c \mathcal{L}_a[\rho(t)], \tag{2}$$

where $\mathcal{L}_a[\rho(t)] = a\rho(t)a^\dagger - \frac{1}{2}[\rho(t)a^\dagger a + a^\dagger a\rho(t)]$ is a standard Lindblad decay term modelling the incoherent decay of the cavity mode due to material and radiative losses. The polaritonic potential energy surfaces used for the interpretation and analysis of the results are obtained by diagonalizing the (undriven) Hamiltonian within the Born-Oppenheimer approximation, i.e., diagonalizing $H(t) - p^2/2$ for $E_0 = 0$ and fixed q [18]. In Figure 1 we show the PoPES within the single-excitation subspace, spanned by the uncoupled states $|e, 0\rangle$ and $|g, 1\rangle$, where $|g\rangle$ ($|e\rangle$) is the electronic ground (excited) state and $|n = 0, 1, \ldots\rangle$ is the cavity mode Fock state with n photons. The Hamiltonian in this subspace can be written as

$$H_{BO}(q) = \begin{pmatrix} \omega_c + \frac{\omega_v^2 q^2}{2} & \Omega_R/2 \\ \Omega_R/2 & \omega_e + \frac{\omega_v^2 q^2}{2} - \lambda_v\sqrt{2\omega_v}q \end{pmatrix}, \tag{3}$$

and diagonalizing it gives the PoPES plotted in Figure 1 and Figure 4(b).

The parameter values chosen for modelling the molecule were based on ab-initio calculations for the anthracene molecule at the TDA-B3LYP level of theory using Gaussian 09 [49]. Fitting the PES obtained in these calculations to a displaced harmonic oscillator model using the Duschinsky linear transformation [50],

$$H_{m,\text{full}} = \omega_e \sigma^+\sigma^- + \sum_k \left[\omega_k b_k^\dagger b_k + \lambda_k(b_k^\dagger + b_k)\right], \tag{4}$$

yields the parameters $\{\omega_k, \lambda_k\}$, or equivalently the spectral density $J_v(\omega) = \sum_k \lambda_k^2 \delta(\omega - \omega_k)$, determining the vibrational spectrum of the molecule. The single vibrational mode in Equation 1 is then taken as the corresponding reaction coordinate, with $\lambda_v = \sqrt{\sum_k \lambda_k^2}$ and $\omega_v = \sum_k \omega_k \lambda_k^2/\lambda_v^2$ [10, 51].

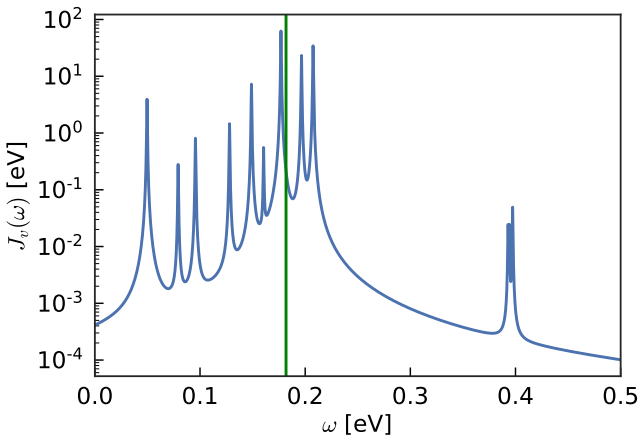

Figure 5. $J_v(\omega)$ for the anthracene molecule. The vertical green line indicates the vibrational frequency ω_v of the reaction coordinate.

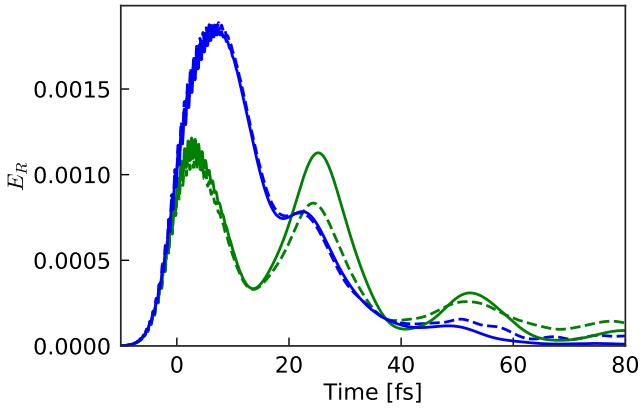

Figure 6. Comparison of the radiative emission between the calculations with a single vibrational mode (full lines) and using TDVMPS calculations (dashed lines) in which the full vibrational spectral density of the molecule is taken into account. In green (blue) the frequency of the laser pulse is $\omega_L = 3.3$ (3.7) eV.

In Figure 5, we show the vibrational spectral density of anthracene (convoluted with a Lorentzian representing broadening due to the interactions with the solid-state environment). It can be seen that ω_v is very close to the frequency of the dominant vibrational mode in $J_v(\omega)$. We have additionally checked the validity of the single-mode approximation by comparing the model calculations above with time-dependent variational matrix product states (TDVMPS) calculations [10, 47] in which the full phononic spectral density, describing all vibrational modes of the molecule and surroundings, is taken into account. The tensor network approach to quantum dynamics relies on the assumption that the ground-state and low-energy excitations live in a corner of the Hilbert space where entanglement is mainly local (entanglement area law). This fact greatly reduces the needed memory allowing for the computation of a quasi-exact solution of the Time-Dependent Schrödinger Equation for systems where a brute force approach is impossible [52].In this fully quantum calculation, vibrational dephasing as well as vibration-driven coupling between polariton modes are accurately represented [10]. As shown in Figure 6, the main features of the signal are conserved for short times, but the presence of the additional vibrational modes leads to dephasing of the coherent wavepacket motion and thus suppression of the oscillations on a timescale of tens of femtoseconds. Studying, e.g., the temperature dependence of the dynamics seen here could thus also allow direct insight into vibrational dephasing of molecular excitations and wavepacket motion in a solid-state environment.

ACKNOWLEDGMENTS

We thank Alex W. Chin and Florian A. Y. N. Schröder for their help with the TDVMPS calculations, and Clàudia Climent for her help with calculating the displaced harmonic oscillator model and with the Duschinsky linear transformation. This work has been funded by the European Research Council grant ERC-2016-STG-714870 and the Spanish Ministry for Science, Innovation, and Universities – AEI grants RTI2018-099737-B-I00, PCI2018-093145 (through the QuantERA program of the European Commission), and MDM-2014-0377 (through the María de Maeztu program for Units of Excellence in R&D).

* ruiefdasilva@gmail.com
† johannes.feist@uam.es

[1] R. J. Thompson, G. Rempe, and H. J. Kimble, Phys. Rev. Lett. **68**, 1132 (1992).
[2] C. Weisbuch, M. Nishioka, A. Ishikawa, and Y. Arakawa, Phys. Rev. Lett. **69**, 3314 (1992).
[3] D. G. Lidzey, D. D. C. Bradley, M. S. Skolnick, T. Virgili, S. Walker, and D. M. Whittaker, Nature **395**, 53 (1998).
[4] G. Zengin, M. Wersäll, S. Nilsson, T. J. Antosiewicz, M. Käll, and T. Shegai, Phys. Rev. Lett. **114**, 157401 (2015).
[5] R. Chikkaraddy, B. de Nijs, F. Benz, S. J. Barrow, O. A. Scherman, E. Rosta, A. Demetriadou, P. Fox, O. Hess, and J. J. Baumberg, Nature **535**, 127 (2016).
[6] O. S. Ojambati, R. Chikkaraddy, W. D. Deacon, M. Horton, D. Kos, V. A. Turek, U. F. Keyser, and J. J. Baumberg, Nat. Commun. **10**, 1049 (2019).
[7] P. Vasa, W. Wang, R. Pomraenke, M. Lammers, M. Maiuri, C. Manzoni, G. Cerullo, and C. Lienau, Nature Photonics **7**, 128 (2013).
[8] P. Törmä and W. L. Barnes, Rep. Prog. Phys. **78**, 013901 (2015).
[9] J. A. Ćwik, P. Kirton, S. De Liberato, and J. Keeling, Phys. Rev. A **93**, 033840 (2016).
[10] J. del Pino, F. A. Y. N. Schröder, A. W. Chin, J. Feist, and F. J. Garcia-Vidal, Phys. Rev. Lett. **121**, 227401 (2018).

[11] F. Herrera and F. C. Spano, ACS Photonics **5**, 65 (2018).
[12] A. Singh, P. M. de Roque, G. Calbris, J. T. Hugall, and N. F. van Hulst, Nano letters **18**, 2538 (2018).
[13] D. M. Coles, N. Somaschi, P. Michetti, C. Clark, P. G. Lagoudakis, P. G. Savvidis, and D. G. Lidzey, Nat. Mater. **13**, 712 (2014).
[14] E. Orgiu, J. George, J. A. Hutchison, E. Devaux, J. F. Dayen, B. Doudin, F. Stellacci, C. Genet, J. Schachenmayer, C. Genes, G. Pupillo, P. Samorì, and T. W. Ebbesen, Nat. Mater. **14**, 1123 (2015).
[15] J. Feist and F. J. Garcia-Vidal, Phys. Rev. Lett. **114**, 196402 (2015).
[16] X. Zhong, T. Chervy, L. Zhang, A. Thomas, J. George, C. Genet, J. A. Hutchison, and T. W. Ebbesen, Angew. Chem. Int. Ed. **56**, 9034 (2017).
[17] J. A. Hutchison, T. Schwartz, C. Genet, E. Devaux, and T. W. Ebbesen, Angew. Chem. **124**, 1624 (2012).
[18] J. Galego, F. J. Garcia-Vidal, and J. Feist, Phys. Rev. X **5**, 041022 (2015).
[19] F. Herrera and F. C. Spano, Phys. Rev. Lett. **116**, 238301 (2016).
[20] A. Thomas, J. George, A. Shalabney, M. Dryzhakov, S. J. Varma, J. Moran, T. Chervy, X. Zhong, E. Devaux, C. Genet, J. A. Hutchison, and T. W. Ebbesen, Angew. Chem. Int. Ed. **55**, 11462 (2016).
[21] J. Flick, M. Ruggenthaler, H. Appel, and A. Rubio, Proc. Natl. Acad. Sci. **114**, 3026 (2017).
[22] B. Munkhbat, M. Wersäll, D. G. Baranov, T. J. Antosiewicz, and T. Shegai, Sci. Adv. **4**, eaas9552 (2018).
[23] J. Fregoni, G. Granucci, E. Coccia, M. Persico, and S. Corni, Nature communications **9**, 4688 (2018).
[24] V. N. Peters, M. O. Faruk, J. Asane, R. Alexander, D. A. Peters, S. Prayakarao, S. Rout, and M. A. Noginov, Optica **6**, 318 (2019).
[25] M. Du, R. F. Ribeiro, and J. Yuen-Zhou, Chem **5**, 1167 (2019).
[26] K. Stranius, M. Hertzog, and K. Börjesson, Nat. Commun. **9**, 2273 (2018).
[27] L. A. Martínez-Martínez, M. Du, R. F. Ribeiro, S. Kéna-Cohen, and J. Yuen-Zhou, J. Phys. Chem. Lett. **9**, 1951 (2018).
[28] A. H. Zewail, J. Phys. Chem. A **104**, 5660 (2000).
[29] F. Krausz and M. Ivanov, Rev. Mod. Phys. **81**, 163 (2009).
[30] E. D. Potter, J. L. Herek, S. Pedersen, Q. Liu, and A. H. Zewail, Nature **355**, 66 (1992).
[31] A. Assion, T. Baumert, M. Bergt, T. Brixner, B. Kiefer, V. Seyfried, M. Strehle, and G. Gerber, Science **282**, 919 (1998).
[32] M. Kling, C. Siedschlag, A. J. Verhoef, J. Khan, M. Schultze, T. Uphues, Y. Ni, M. Uiberacker, M. Drescher, F. Krausz, *et al.*, Science **312**, 246 (2006).
[33] M. E. Corrales, J. González-Vázquez, G. Balerdi, I. R. Solá, R. de Nalda, and L. Bañares, Nat. Chem. **6**, 785 (2014).
[34] A. Palacios and F. Martín, Wiley Interdisciplinary Reviews: Computational Molecular Science , doi: 10.1002/wcms.1430 (2019).
[35] M. Kowalewski, K. Bennett, and S. Mukamel, J. Phys. Chem. Lett. **7**, 2050 (2016).
[36] O. Vendrell, Chem. Phys. **509**, 55 (2018).
[37] J. F. Triana and J. L. Sanz-Vicario, Phys. Rev. Lett. **122**, 063603 (2019).
[38] J. Feist, J. Galego, and F. J. Garcia-Vidal, ACS Photonics **5**, 205 (2018).
[39] C. Iaconis and I. A. Walmsley, Opt. Lett., OL **23**, 792 (1998).
[40] R. Trebino, K. W. DeLong, D. N. Fittinghoff, J. N. Sweetser, M. A. Krumbügel, B. A. Richman, and D. J. Kane, Review of Scientific Instruments **68**, 3277 (1997).
[41] M. Miranda, C. L. Arnold, T. Fordell, F. Silva, B. Alonso, R. Weigand, A. L'Huillier, and H. Crespo, Opt. Express **20**, 18732 (2012).
[42] P. Michetti and G. C. La Rocca, Phys. Rev. B **79**, 035325 (2009).
[43] P. Kirton and J. Keeling, Phys. Rev. Lett. **111**, 100404 (2013).
[44] F. C. Spano, J. Chem. Phys. **142**, 184707 (2015).
[45] S. Kéna-Cohen and S. R. Forrest, Nat. Photonics **4**, 371 (2010).
[46] M. Ramezani, A. Halpin, A. I. Fernández-Domínguez, J. Feist, S. R.-K. Rodriguez, F. J. Garcia-Vidal, and J. Gómez Rivas, Optica **4**, 31 (2017).
[47] F. A. Y. N. Schröder, D. H. P. Turban, A. J. Musser, N. D. M. Hine, and A. W. Chin, Nat. Commun. **10**, 1062 (2019).
[48] G. P. Acuna, F. M. Möller, P. Holzmeister, S. Beater, B. Lalkens, and P. Tinnefeld, Science **338**, 506 (2012).
[49] M. J. Frisch, G. W. Trucks, H. B. Schlegel, G. E. Scuseria, M. A. Robb, J. R. Cheeseman, G. Scalmani, V. Barone, G. A. Petersson, H. Nakatsuji, X. Li, M. Caricato, A. Marenich, J. Bloino, B. G. Janesko, R. Gomperts, B. Mennucci, H. P. Hratchian, J. V. Ortiz, A. F. Izmaylov, J. L. Sonnenberg, D. Williams-Young, F. Ding, F. Lipparini, F. Egidi, J. Goings, B. Peng, A. Petrone, T. Henderson, D. Ranasinghe, V. G. Zakrzewski, J. Gao, N. Rega, G. Zheng, W. Liang, M. Hada, M. Ehara, K. Toyota, R. Fukuda, J. Hasegawa, M. Ishida, T. Nakajima, Y. Honda, O. Kitao, H. Nakai, T. Vreven, K. Throssell, J. A. Montgomery, Jr.,, J. E. Peralta, F. Ogliaro, M. Bearpark, J. J. Heyd, E. Brothers, K. N. Kudin, V. N. Staroverov, T. Keith, R. Kobayashi, J. Normand, K. Raghavachari, A. Rendell, J. C. Burant, S. S. Iyengar, J. Tomasi, M. Cossi, J. M. Millam, M. Klene, C. Adamo, R. Cammi, J. W. Ochterski, R. L. Martin, K. Morokuma, O. Farkas, J. B. Foresman, and D. J. Fox, "Gaussian 09, Revision E.01," Gaussian, Inc (2009).
[50] F. Duschinsky, Acta Physicochimica URSS **7**, 551 (1937).
[51] A. W. Chin, Á. Rivas, S. F. Huelga, and M. B. Plenio, J. Math. Phys. **51**, 092109 (2010).
[52] U. Schollwöck, Annals of Physics **326**, 96 (2011).